Supporting Information for

Adjustable magnetoresistance in semiconducting carbonized phthalonitrile resin

Chong Gao,[a] Ming Yang,[e] Wenhao Xie,[a,d] Hang Zhang,[e] Hongbo Gu,*[,a] Ai Du,[f] Zhong Shi,[f] Ying Guo,[b] Heng Zhou,*[,b] Zhanhu Guo*[,c]

[a]Shanghai Key Lab of Chemical Assessment and Sustainability, School of Chemical Science and Engineering, Tongji University, Shanghai 200092, People's Republic of China

[b]Institute of Chemistry, Chinese Academy of Sciences, Beijing 100190, China

[c]Integrated Composites Lab (ICL), Department of Chemical & Biomolecular Engineering University of Tennessee, Knoxville, TN, 37966, USA

[d]Key Laboratory of Materials Processing and Mold (Zhengzhou University), Ministry of Education, National Engineering Research Center for Advanced Polymer Processing Technology, Zhengzhou University, Zhengzhou, China

[e]Institute of Engineering Thermophysics, Chinese Academy of Sciences, Beijing 100049, China

[f]Shanghai Key Laboratory of Special Artificial Microstructure Materials and Technology, School of Physics Science and Engineering, Tongji University, Shanghai 200092, China

*Corresponding author

E-mail: hongbogu2014@tongji.edu.cn;
zhouheng@iccas.ac.cn;
zguo10@utk.edu

Chemical structure of 2,2-bis[4-(3,4-dicyanophenoxy)phenyl] hexafluoropropane (FPN):

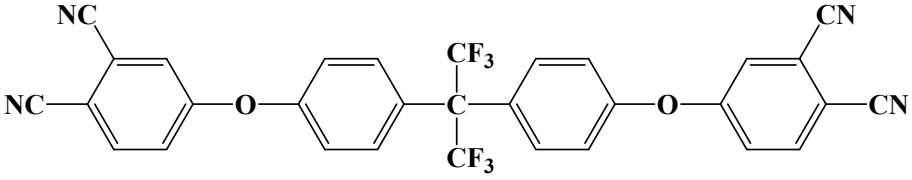

Chemical structure of PANI:

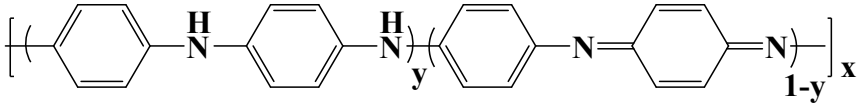

Experimental Section

Materials. 4-nitrophthalonitrile (NPN, ≥98.0%) was purchased from Alpha Chemical Co., Ltd (Shijiazhuang, China) and used after recrystallization from ethanol. 4,4'-(hexafluoroisopropylidene)diphenol (bisphenol AF) was supplied by Xinhua Chemicals (Suzhou, China), and used without further purification. Resorcinol ($C_6H_6O_2$, 99%) and sodium hydroxide (NaOH, ≥96.0%) was purchased from Sinopharm Chemicals (Shanghai, China) and used without further purification. N,N-dimethylformamide (DMF, ≥99.0%), from Beijing Beihua Fine Chemicals Co., was purified by distillation over phosphorus pentoxide under reduced pressure. Anhydrous potassium carbonate (K_2CO_3, 99%) and hydrochloric acid (HCl, 36-38 wt%) were utilized as received from Beijing Beihua Fine Chemicals Co., China. 4-aminophenol (C_6H_7NO, 99.5%) was bought from Aladdin Reagent Company (China). Distilled water was made by twice distillation.

Preparation of 2,2-bis[4-(3,4-dicyanophenoxy)phenyl] hexafluoropropane (FPN). The synthesis of FPN was conducted according to a modified Keller's method.[1] Briefly, 67.25 g (0.20 mol) of bisphenol AF, 72.71 g (0.42 mol) of 4-nitrophthalonitrile

and 400 mL of DMF were added into a three-neck round-bottom flask equipped with a condenser, a thermometer and a nitrogen inlet under the magnetic stirring. When the above mixture became homogenous, 55.28 g (0.40 mol) of anhydrous K_2CO_3 was added. Then the mixture was gently heated to 80 ^oC, and stirred for 6 h under the nitrogen atmosphere. Upon cooling down to room temperature, the resulting dark brown mixture was poured into 0.1 mol/L of hydrochloric acid solution, filtered and washed with distilled water to neutral. After drying in a vacuum oven, the 108.28 g of product was obtained and the yield is 92%. Melting point: 233.0 ^oC (determined by differential scanning calorimetry (DSC)). The detailed characterization shows as follows:

^1H nuclear magnetic resonance (^1H-NMR, 400 MHz, DMSO-d_6, δ): 8.16 (d, J=8.7 Hz, 2H), 7.96 (d, J=2.5 Hz, 2H), 7.54 (dd, J=8.7, 2.5 Hz, 2H), 7.49 (d, J=8.6 Hz, 4H), 7.31 (d, J=9.0 Hz, 2H).

FTIR (cm^{-1}, ν): 2236 (-CN), 1248 (-C-O-C-), 1122 (-CF_3)

Preparation of 4-(4-Aminophenoxy) phthalonitrile (APN). APN was prepared according to our previous study.[2] 17.3 g (0.10 mol) 4-nitrophthalonitrile, 10.9 g (0.10 mol) of 4-aminophenol, and 50 mL of DMF were added into a 250 mL of three-neck round-bottom flask . After they were dissolved, anhydrous K_2CO_3 (20.7 g, 0.15 mol) was put into the above mixture. The mixture was magnetically stirred at 85 ^oC for 5 h under the nitrogen atmosphere. After cooling down to room temperature, the resulting dark brown mixture was poured into 0.1 mol/L of NaOH solution, the resultant precipitate was collected by filtration and washed with deionized water until pH was about 7. The product was dried at 80 ^oC in a vacuum oven overnight.

Preparation of carbonized FPN/APN resins. Firstly, the FPN/APN resin was prepared according to the literature report.[3] In brief, 10 g of FPN was added into a three-neck round-bottom flask and heated to 160 °C. When the FPN monomer is completely melted, 0.6 g of APN (weight percentage of APN was 6%) was added into the system. After 5 min of magnetic stirring, the melting blends were poured into a silicone mould and placed in an oven with the curing sequences of 200 °C for 4 h, 250 °C for 4 h, 280 °C for 6 h and 300 °C for 6 h to attain the FPN/APN resin. The proposed curing mechanism of FPN resin is drawn in Scheme S1. Then, the FPN/APN resins were placed in a tube furnace (GSL-1100X-S, Kejing Co. Ltd., Hefei, China) at 550 °C for 8 h followed by processing in an infrared furnace (Beijing Huace Testing Instrument Co., Ltd.) with the heating sequences of 600 °C for 20 min, 700 °C for 20 min, and 800 °C for 20 min to obtain the graphite-like FPN/APN resin, labeled as 6FPN-800. The graphite-like FPN/APN resin with 3 and 10% weight percentage of APN (named as 3FPN and 10FPN) were also fabricated with the same process for comparison. To explore the relationship between MR phenomenon and annealing temperature, the 6% weight percentage of FPN/APN resin was placed in the infrared furnace annealing at 600 °C for 20 min named as 6FPN-600. Afterwards, the 6FPN-600 was further annealing at 700 °C for 20 min to obtain the sample of 6FPN-700. The 6FPN-800-40 was prepared by annealing at 800 °C for 40 min based on 6FPN-700.

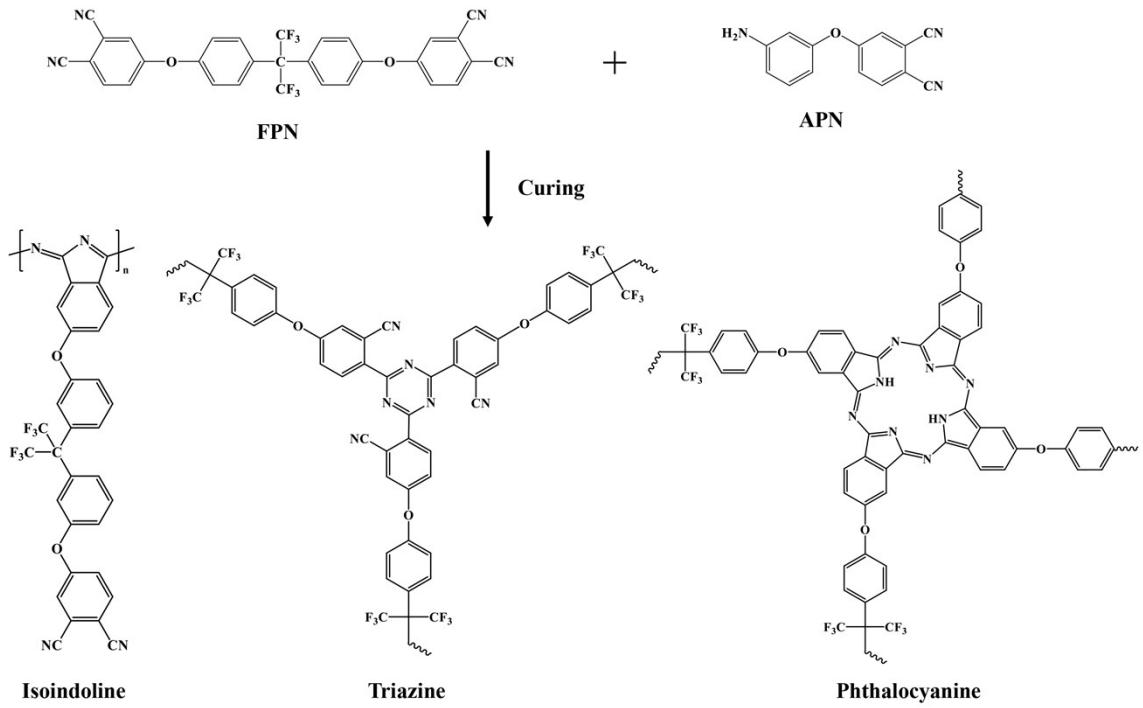

Scheme S1 Proposed curing mechanism of FPN resin.

Characterizations. Fourier transform infrared spectroscopy (FTIR) coupled with an attenuated total reflection (ATR) accessory (Bruker Inc. Vector 22) was applied to characterize the chemical structure of cured FPN/APN resins in the range of 500 to 3000 cm^{-1} at a resolution of 2 cm^{-1}. Raman spectroscopy was carried out on an Invia micro-Raman spectrometer (Renishaw Company, UK, spectral region: 400-3200 cm^{-1}). The X-ray diffraction (XRD) of products was obtained on a D8 Advance X-ray powder diffractometer, Bruker Company, Germany (40 kV, 40 mA) with a scanning range from 10 to 70 °. The microstructures of the synthesized products were reviewed on a scanning electron microscope (SEM, Hitachi S-4800 system). X-ray photoelectron spectroscopy (XPS) analysis was carried out using a Kratos AXIS Ultra DLD spectrometer with Al Kα ($h\nu$ = 1486.6 eV) radiation as the excitation source at an anode voltage of 12 kV and an emission current of 10 mA. Solid-state ^{13}C NMR spectra were measured on a Bruker

Avance III 400 spectrometer with cross-polarization magic angle spinning. Magnetoresistance was carried out using a standard four-probe technique by a 9-Tesla Physical Properties Measurement System (PPMS) by Quantum Design at room temperature, in which the magnetic field was perpendicular to the current.

First-principle calculations and finite temperature molecular dynamics (FTMD) simulations. To obtain the microscopic atomic positions and verify the lattice stabilities, we have performed the first-principle calculations and the finite temperature molecular dynamics (FTMD) simulations. The initial lattice structures for triazine, phthalocyanine and isoindoline constructed by ChemDraw are shown in Fig. S1(a-c). A vacuum layer of 15 Å along *c*-axis was added so that the molecular would not interact with itself along with this direction. Then, geometrical optimizations were proceeded in the framework of the generalized gradient approximation (GGA) based on the density functional theory (DFT). In such calculations, Vienna ab initio simulation package (VASP) was utilized.[4-6] The generalized gradient approximation[7] as parameterized by Perdew-Burke-Ernzerhof (PBE) was used in the form of exchange correlation functional. The plane-wave cutoff energies were set as 370 eV. The atomic positions were fully optimized by the conjugated gradient algorithm while the Hellmann-Feynman force convergence threshold of 0.01 eV/Å was set as the break condition for the ionic relaxation loop. In order to further verify the stability of these materials, we have also conducted the finite temperature molecular dynamics (FTMD) simulations at different temperatures.

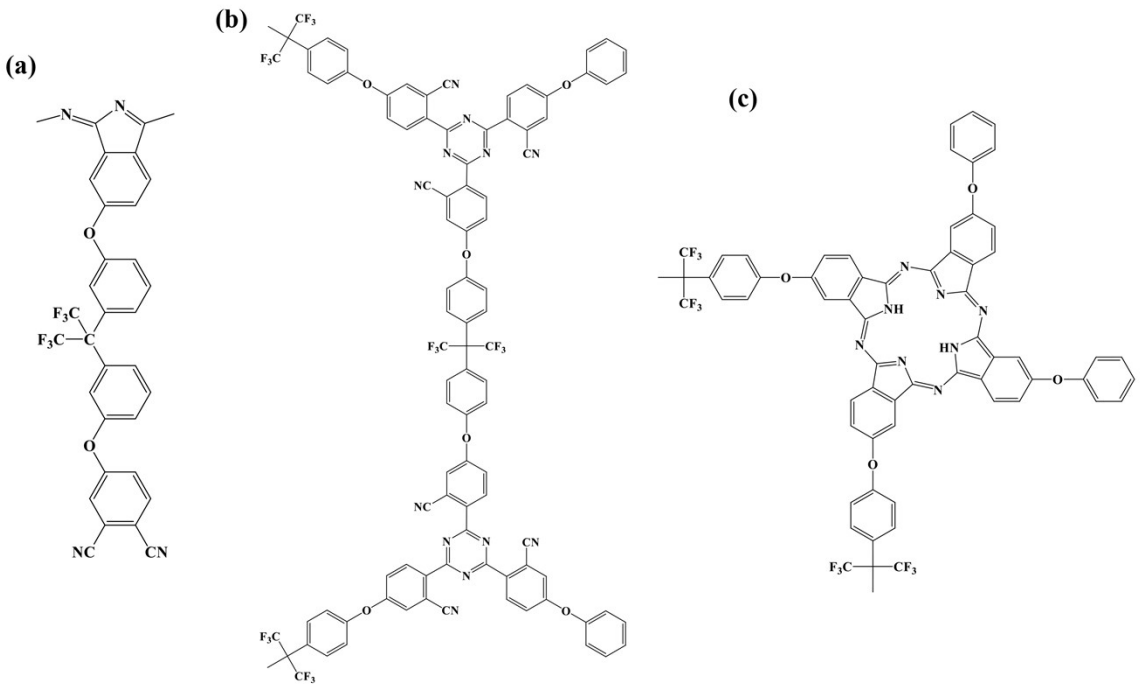

Fig. S1 Initial lattice structures for (a) isoindoline, (b) triazine and (c) phthalocyanine.

Scanning electron microscope (SEM)

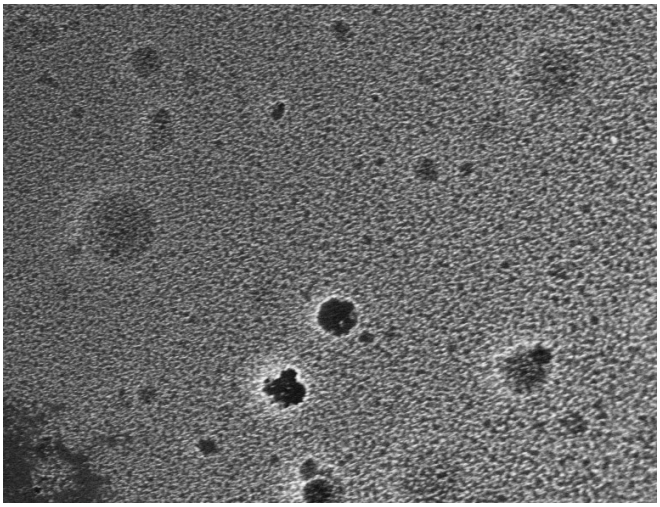

Fig. S2 SEM image of surface of 6FPN-800.

Fourier transform infrared spectroscopy (FTIR)

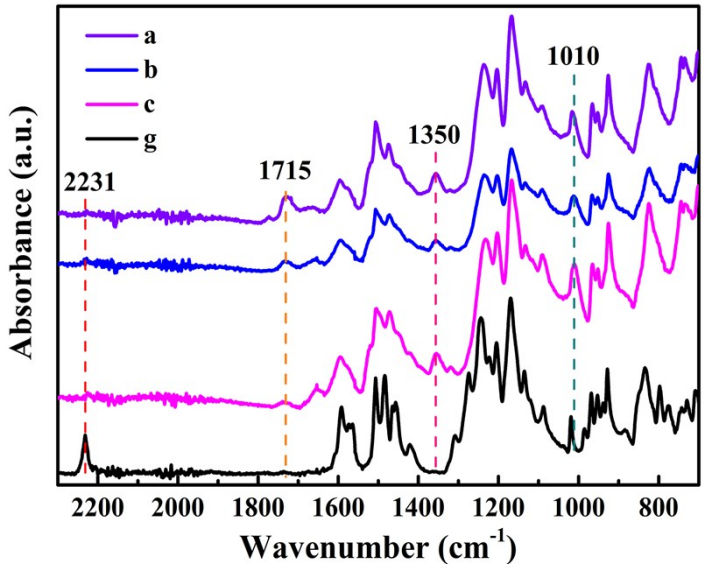

Fig. S3 FTIR spectra of (a) 3FPN-800, (b) 6FPN-800, (c) 10FPN-800, and (g) FPN.

To investigate the main structures of FPN/APN resins, their chemical structures after being cured have been studied by FTIR spectroscopy, as shown in Fig. S3. It's worth noting that the characteristic absorption band at 2231 cm^{-1} in the FTIR spectrum of FPN, Fig. S3(g), belongs to the stretching vibration of cyano group, which is hard to be seen in the FTIR spectrum of those cured FPN/APN resins. The apparent peaks corresponding to the stretching vibration of triazine (1350 cm^{-1}) and phthalocyanine structure (1010 cm^{-1}) could be observed in the FTIR spectra for all the cured FPN/APN resins, implying the curing of FPN/APN resins. The absorption peak at 1715 cm^{-1} is assigned to the stretching vibration of isoindoline structure, and its peak intensity is declined with increasing the weight percentage of APN from of 3 to 10% in the cured FPN/APN resin system, Fig. S3(a-c).

XPS and ^{13}C NMR of 6FPN-600

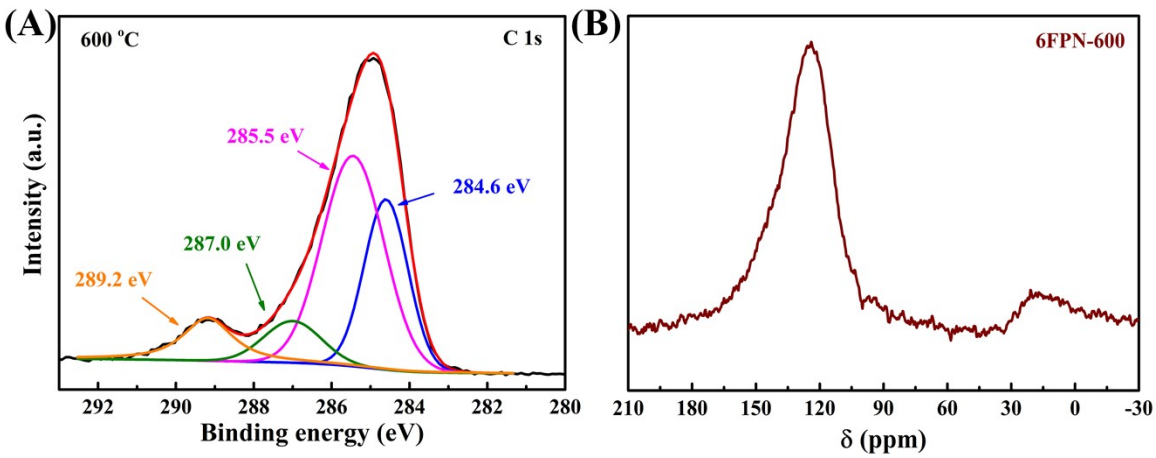

Fig. S4 (A) High resolution of C 1s XPS spectrum and (B) ^{13}C NMR of 6FPN-600.

Raman spectroscopy

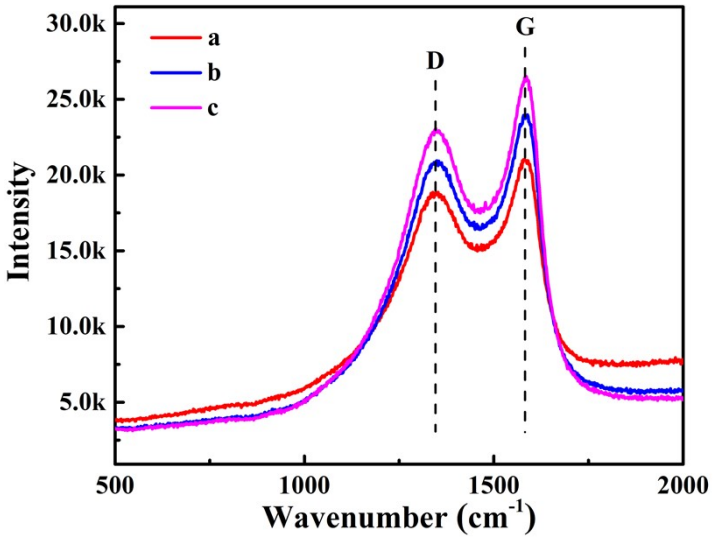

Fig. S5 Raman spectra of (a) 3FPN-800, (b) 6FPN-800, (c) 10FPN-800.

Fig. S5 illustrates the Raman spectra of 3FPN-800, 6FPN-800, and 10FPN-800. Two remarkable peaks at 1350 and 1580 cm^{-1} are noticed in the Raman spectrum for these three samples, which is correlated with the D (that is attributed to the amorphous carbon and defects) and G (that is related to E_{2g} vibrational mode

of the *sp*) bands, accordingly. The intensity ratio of D and G bands (I_D/I_G) for 3FPN-800, 6FPN-800, and 10FPN-800 are 1.98, 1.89, and 1.97, respectively. There is no distinct difference in the degree of graphitization for these samples.

Computational results

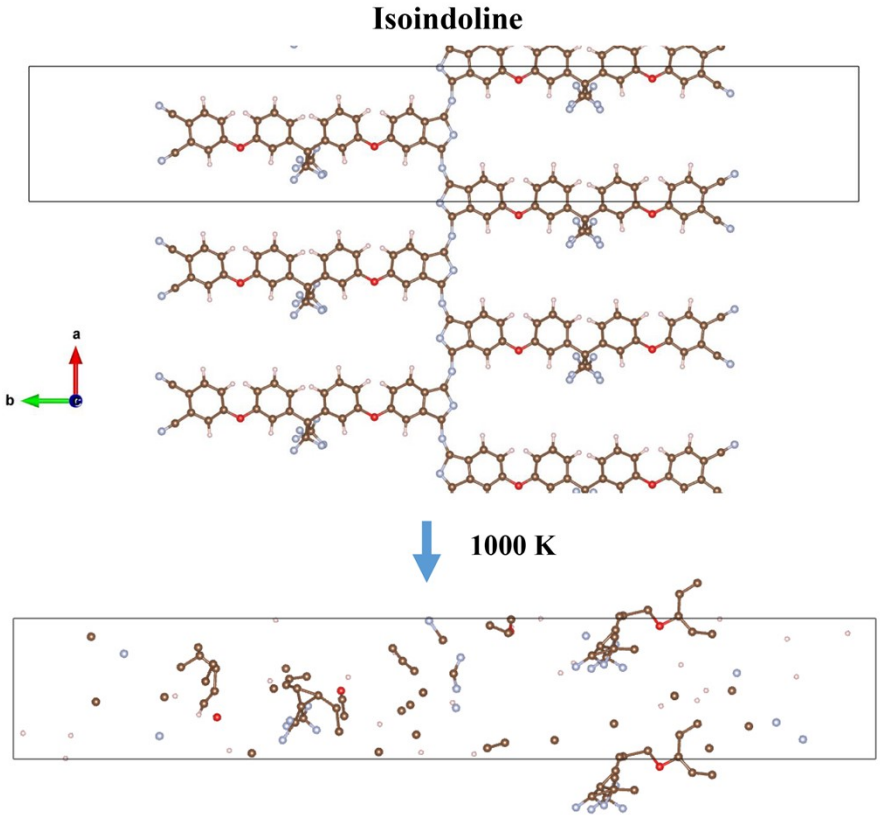

Fig. S6 Initial structure of polyisoindoline and computational results after annealing at 1000 K.

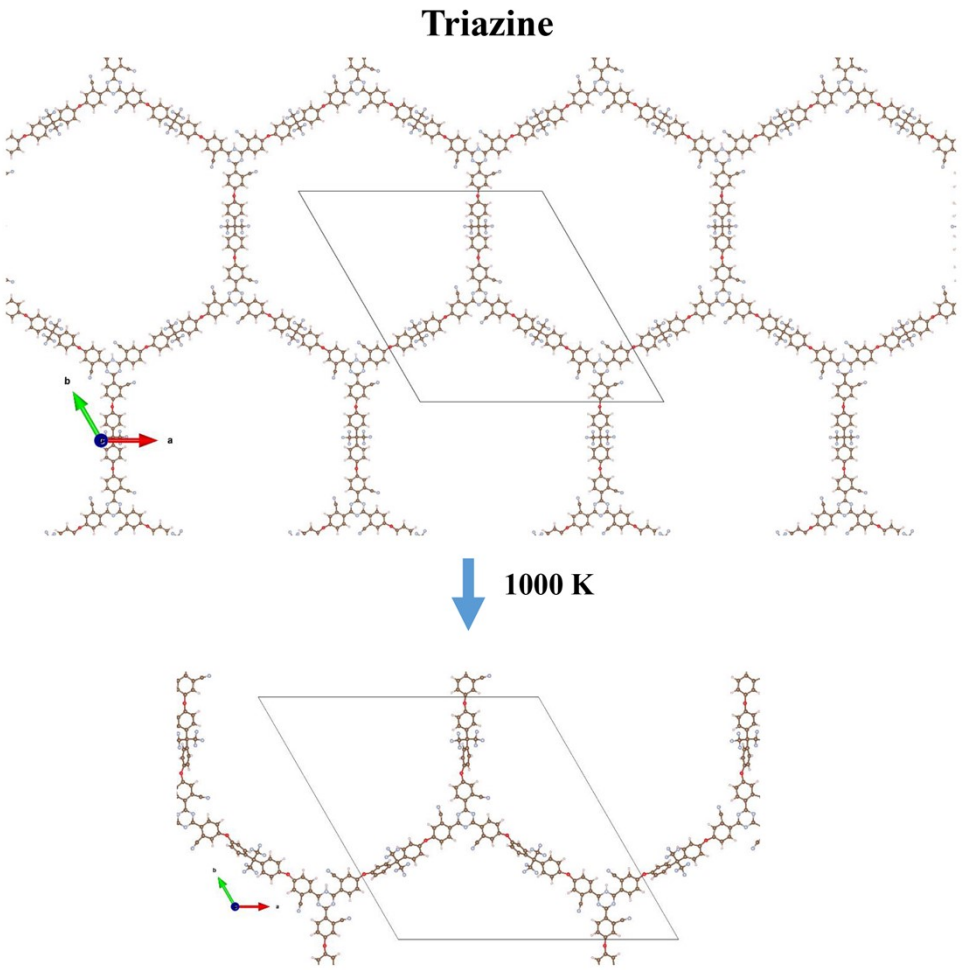

Fig. S7 Initial structure of polytriazine and computational results after annealing at 1000 K.

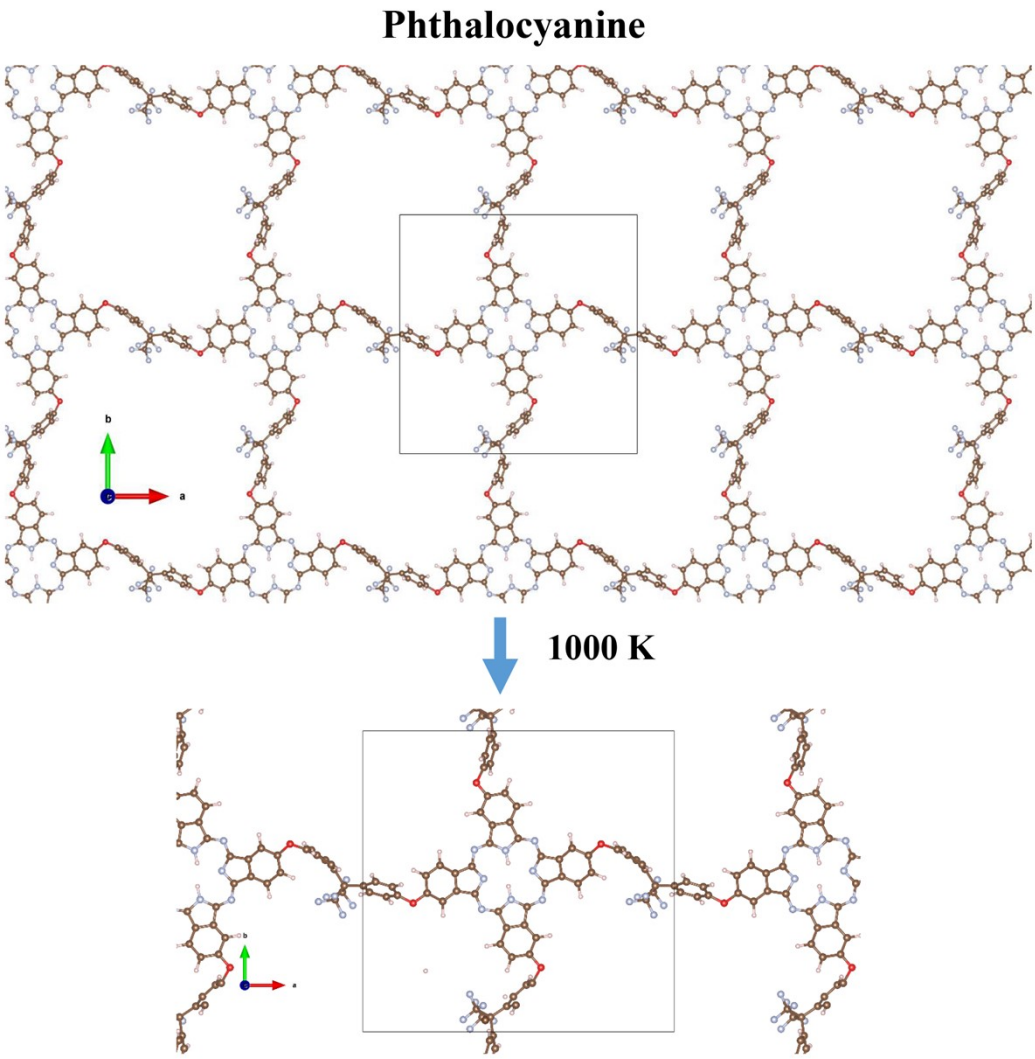

Fig. S8 Initial structure of polyphthalocyanine and computational results after annealing at 1000 K.

According to the above computational results, it is easy to see that the structure of polyisoindoline is completely degraded at 1000 K, whereas the polyphthalocyanine structure has a little bit change with losing some hydrogen atoms and the polytriazine structure almost has no change. Consequently, we could conclude that the polytriazine and polyphthalocyanine are relatively stable after annealing and they are the main structures in the carbonized FPN/AN resins. The charge carrier transfer could only occur in these polytriazine and polyphthalocyanine structures. The proposed schematic diagram

for charge transfer mechanism in semiconducting carbonized FPN/APN resin is depicted in Fig. S9.

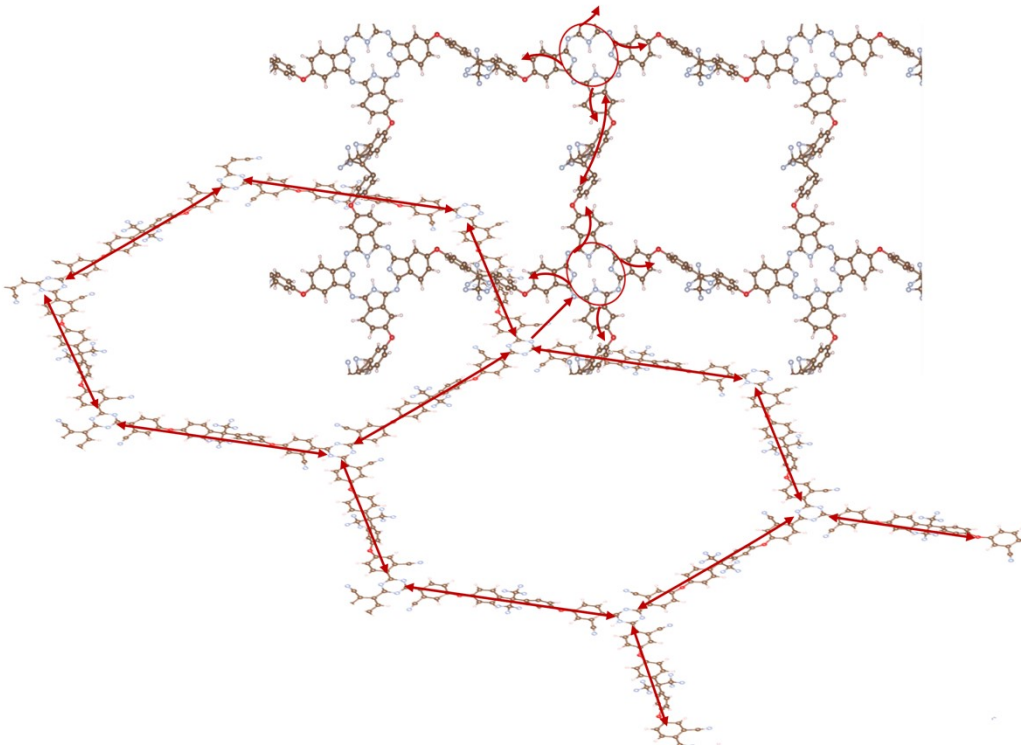

Fig. S9 Proposed schematic diagram for charge transfer mechanism in semiconducting carbonized FPN/APN resin.

Charge carrier transport model:

It is worth mentioning that we have observed an outstanding MR effect in these carbonized FPN/APN resins. The MR is measured on a PPMS system and is calculated by eqn (S1)

$$\mathrm{MR}\% = \frac{R(H) - R(0)}{R(0)} \times 100\% \qquad \text{(S1)}$$

where $R(H)$ and $R(0)$ represent the resistance of materials under and without a magnetic field.

Within the temperature range of 100-180 K, the Mott VRH mechanism is applied to analyze the transport mechanism of charge carriers by following eqn (S2):

$$\sigma = \sigma_0 \exp\left[-\left(\frac{T_0}{T}\right)^{1/(n+1)}\right], \quad n = 1,\ 2,\ 3 \tag{S2}$$

where the σ_0 is a constant representing the conductivity of the sample at the infinite high temperature and T_0 is the Mott characteristic temperature. The value of n is 1, 2, and 3, corresponding to three different models (Efros-Shklovskii variable range hopping (ES-VRH), 2D, and 3D VRH models, accordingly).[8] The obtained σ_0 and T_0 are listed in Table S1. From Table S1, it's seen that both T_0 and σ_0 of carbonized FPN/APN resins are decreased apparently as the processing temperature increases.

The thermally activated transport (TAT) model is accepted in the temperature range from 180-290 K to investigate the electrical properties of graphite-like FPN/APN resin as shown in eqn (S3):

$$R(T) = R_0 \exp\left(\frac{E}{k_B T}\right) \tag{S3}$$

where R_0 is a constant, k_B is the Boltzmann constant, and the E is related to the activation energy.[9] The Mott VRH model and TAT model are the possible suitable mechanisms for explaining the resistivity and temperature relationship for all the carbonized FPN/APN systems.

Wave-function shrinkage model:

In the wave-function shrinkage model, the relationship between MR and magnetic field could be explained by eqn (S4):[10]

$$\mathrm{MR} = \frac{R(H,T) - R(0,T)}{R(0,T)} \approx t\frac{H^2}{P_C^2}\left(\frac{T_0}{T}\right)^{1/4} = t\frac{e^2 a_0^4}{36\hbar^2}(\frac{T_0}{T})^{3/4} H^2 \quad \text{(S4)}$$

where t is a numerical constant (=5/2016), H is the magnetic field, P_c is the normalized characteristic magnetic field and could be expressed by eqn (S5):

$$P_C = 6\hbar/[ea_0^2(T_0/T)^{1/4}] \quad \text{(S5)}$$

where e is electron charge, $\hbar$ is the reduced Planck's constant, a_0 is the localization length, and T_0 is the Mott characteristic temperature (K). It is easy to see that the MR value obtained from eqn (S4) should be positive, so the wave-function shrinkage model is always used to analyze the positive MR value. According to eqn (S4), the a_0 at different magnetic field could be obtained by the eqn (S6):

$$a_0^4 = \frac{36\hbar^2 \mathrm{MR}}{t_2 e^2}(\frac{T_0}{T})^{-3/4} H^{-2} \quad \text{(S6)}$$

And the obtained a_0 for samples with a positive MR value are listed in Table S2.

Forward interference model:

In the forward interference model, the ratio $R(H,T)/R(0,T)$ caused by the interference effects is described by empirical eqn (S7), which neglects the quadratic term in H:[11]

$$R(H,T)/R(0,T) \approx 1/\{1 + C_{\mathrm{sat}}[H/H_{\mathrm{sat}}]/[1 + H/H_{\mathrm{sat}}]\} \quad \text{(S7)}$$

where the fitting parameter C_{sat} is a constant and the other fitting parameter H_{sat} is the effective magnetic field to saturate the MR. By fitting $R(H)/R(0) \sim H$ *via* eqn (S7) by using Polymath software, the obtained C_{sat} value for 6FPN-800 is 0.1134.

For the Mott VRH electrical conduction mechanism, H_{sat} is given by eqn (S8):[12]

$$H_{sat} \approx 0.7\left(\frac{8}{3}\right)^{3/2}\left(\frac{1}{a_0^2}\right)\left(\frac{h}{e}\right)\left(\frac{T}{T_0}\right)^{3/8} \quad \text{(S8)}$$

where h is Planck's constant, e is electron charge and T_0 is the Mott characteristic temperature (K). In the low-field limit, eqn (S7) becomes eqn (S9).

$$R(H,T)/R(0,T) \approx 1 - C_{sat}[H/H_{sat}] \quad \text{(S9)}$$

Substituting eqn (S8) into eqn (S9) and rearranging, the obtained MR is as eqn (S10).

$$MR = \frac{R(H,T)-R(0,T)}{R(0,T)} \approx -C_{sat}[H/H_{sat}] = -C_{sat}\frac{H}{0.7\left(\frac{8}{3}\right)^{3/2}\left(\frac{1}{a_0^2}\right)\left(\frac{h}{e}\right)\left(\frac{T}{T_0}\right)^{3/8}} \quad \text{(S10)}$$

The obtained localization length a_0 at different H for the samples with the negative MR value is calculated from eqn (S10) and also listed in Table S2.

In the VRH electrical conduction mechanism, the average hopping length (R_{hop}) is related to the distance that the charge carriers could hop. And the density of states at the Fermi level ($N(E_F)$) determines the hopping probability of charge carriers between the localized states. Both R_{hop} and $N(E_F)$ are important parameters to explain the transport of charge carriers, and they can be revealed by eqns. (11) and (12):

$$R_{hop} = \frac{3}{8}\left(\frac{T_0}{T}\right)^{1/4} a_0 \quad \text{(S11)}$$

$$N(E_F) = \frac{24}{\pi k_B T_0 a_0^3} \quad \text{(S12)}$$

where k_B is Boltzmann constant. The obtained R_{hop} and $N(E_F)$ for all samples is listed in Table S2 as well.

Table S1. R_0, E, σ_0 and T_0 for the graphite-like FPN/APN resins.

Samples	R_0 (Ω cm)	E (meV)	r^2 (TAT)	σ_0 (S cm^{-1})	T_0 (K)	r^2 (VRH)
6FPN-600	1.72	140.30	0.9999	1.30×10^{11}	2.74×10^{8}	0.9999
6FPN-700	5.28×10^{-1}	77.20	0.9993	4.26×10^{6}	2.65×10^{7}	0.9991
6FPN-800	5.71×10^{-2}	32.41	0.9993	2.91×10^{3}	4.78×10^{5}	0.9996

Table S2. Calculated parameters from wave-function shrinkage model and forward interference model.

Samples	Parameters	Magnetic field H (T)		
		0.3	**2.7**	**9**
6FPN-600	a_0 (nm)	10.91	5.18	3.13
	R_{hop} (nm)	127.57	60.53	36.54
	$N(E_F)$ ((J cm^3)$^{-1}$)	1.55×10^{33}	1.46×10^{34}	6.61×10^{34}
6FPN-700	a_0 (nm)	8.06	4.13	2.86
	R_{hop} (nm)	52.54	26.90	18.63
	$N(E_F)$ ((J cm^3)$^{-1}$)	3.99×10^{34}	2.97×10^{35}	8.96×10^{35}
6FPN-800	a_0 (nm)	17.36	12.65	8.23
	R_{hop} (nm)	36.89	26.89	17.49
	$N(E_F)$ ((J cm^3)$^{-1}$)	2.21×10^{35}	5.71×10^{35}	2.07×10^{36}

In contrast, after prolongation of annealing time to 40 min, the 6FPN-800-40 sample does not exhibit obvious MR property (only 1.1%), Fig. 1B(f). In fact, the unpaired electrons (or spins) play an important role in the MR effect.[13, 14] It's reported that during the annealing, more and more unpaired electrons are formed and eventually reach a certain concentration level in the PN resin, which is beneficial for producing MR effect. However, after annealing at 800 °C for a long time, the 6FPN-800-40 sample may possess more stable and ordered structures, leading to the reduce of unpaired electrons (or spins) and weak MR effect.

References:

1. Y. Han, D. Tang, G. Wang, Y. Zhang, Y. Guo, H. Zhou, W. Qiu and T. Zhao, *Polymer*, 2019, **173**, 88-102.
2. B.-G. Sun, H.-Q. Shi, K.-X. Yang, Q. Lei, Y.-Q. Li, Y.-Q. Fu, N. Hu, Y. Guo, H. Zhou and S.-Y. Fu, *Compos. Commun.*, 2020, **18**, 55-61.
3. C. Gao, H. B. Gu, A. Du, H. Zhou, D. Pan, N. Naik and Z. H. Guo, *Polymer*, 2021, **219**, 123533.
4. G. Kresse and J. Hafner, *Phys. Rev. B*, 1994, **49**, 14251-14269.
5. G. Kresse and J. Furthmuller, *Phys. Rev. B*, 1996, **54**, 11169-11186.
6. G. Kresse and J. Furthmuller, *Comp. Mater. Sci.*, 1996, **6**, 15-50.
7. J. P. Perdew, K. Burke and M. Ernzerhof, *Phys. Rev. Lett.*, 1996, **77**, 3865-3868.
8. J. Y. Cai, W. X. Wang, D. Pan, D. P. Young, H. B. Gu and Z. H. Guo, *J. Phys. Chem. C*, 2020, **124**, 22646-22655.
9. J. Guo, X. Li, H. Liu, D. P. Young, G. Song, K. N. Song, J. F. Zhu, J. Kong and Z. H. Guo, *Adv. Compos. Hybrid Mater.*, 2021, **4**, 51-64.
10. H. Gu, J. Guo, H. We, Y. Huang, C. Zhao, Y. Li, Q. Wu, N. Haldolaarachchige, D. P. Young, S. Wei and Z. Guo, *Phys. Chem. Chem. Phys.*, 2013, **15**, 10866-10875.
11. T. Iwasaki, S. Nakamura, O. G. Agbonlahor, M. Muruganathan, M. Akabori, Y. Morita, S. Moriyama, S. Ogawa, Y. Wakayama, H. Mizuta and S. Nakaharai, *Carbon*, 2021, **175**, 87-92.
12. H. Gu, J. Guo, X. Zhang, Q. He, Y. Huang, H. A. Colorado, N. S. Haldolaarachchige, H. L. Xin, D. P. Young, S. Wei and Z. Guo, *J. Phys. Chem. C*, 2013, **117**, 6426-6436.
13. T. M. Keller, *J. Polym. Sci., Part A: Polym. Chem.*, 1987, **25**, 2569-2576.
14. H. Gu, X. Xu, J. Cai, S. Wei, H. Wei, H. Liu, D. Young, Q. Shao, S. Wu, T. Ding and Z. Guo, *Chem. Commun.*, 2019, **55**, 10068-10071.